MIT Open Access Articles

The Formation of Magnetic Depletions and Flux Annihilation Due to Reconnection in the Heliosheath

The MIT Faculty has made this article openly available. ***Please share*** how this access benefits you. Your story matters.

Citation	Drake, J. F.; Swisdak, M.; Opher, M. and Richardson, J. D. "The Formation of Magnetic Depletions and Flux Annihilation Due to Reconnection in the Heliosheath." The Astrophysical Journal 837, no. 2 (March 2017): 159 © 2017 The American Astronomical Society
As Published	http://dx.doi.org/10.3847/1538-4357/aa6304
Publisher	IOP Publishing
Version	Final published version
Citable link	http://hdl.handle.net/1721.1/109540
Terms of Use	Article is made available in accordance with the publisher's policy and may be subject to US copyright law. Please refer to the publisher's site for terms of use.

Massachusetts Institute of Technology

DSpace@MIT

The Astrophysical Journal, 837:159 (9pp), 2017 March 10 https://doi.org/10.3847/1538-4357/aa6304
© 2017. The American Astronomical Society. All rights reserved.

The Formation of Magnetic Depletions and Flux Annihilation Due to Reconnection in the Heliosheath

J. F. Drake[1,2], M. Swisdak[2], M. Opher[3], and J. D. Richardson[4]
[1] Department of Physics, the Institute for Physical Science and Technology and the Joint Space Institute, University of Maryland, College Park, MD 20742, USA; drake@umd.edu
[2] Institute for Research in Electronics and Applied Physics, University of Maryland, College Park, MD 20742, USA
[3] Astronomy Department, Boston University, MA 02215, USA
[4] Kavli Center for Astrophysics and Space Science, Massachusetts Institute of Technology, Cambridge, MA 02139, USA
Received 2016 December 21; revised 2017 February 21; accepted 2017 February 22; published 2017 March 15

Abstract

The misalignment of the solar rotation axis and the magnetic axis of the Sun produces a periodic reversal of the Parker spiral magnetic field and the sectored solar wind. The compression of the sectors is expected to lead to reconnection in the heliosheath (HS). We present particle-in-cell simulations of the sectored HS that reflect the plasma environment along the *Voyager 1* and *2* trajectories, specifically including unequal positive and negative azimuthal magnetic flux as seen in the *Voyager* data. Reconnection proceeds on individual current sheets until islands on adjacent current layers merge. At late time, bands of the dominant flux survive, separated by bands of deep magnetic field depletion. The ambient plasma pressure supports the strong magnetic pressure variation so that pressure is anticorrelated with magnetic field strength. There is little variation in the magnetic field direction across the boundaries of the magnetic depressions. At irregular intervals within the magnetic depressions are long-lived pairs of magnetic islands where the magnetic field direction reverses so that spacecraft data would reveal sharp magnetic field depressions with only occasional crossings with jumps in magnetic field direction. This is typical of the magnetic field data from the *Voyager* spacecraft. *Voyager 2* data reveal that fluctuations in the density and magnetic field strength are anticorrelated in the sector zone, as expected from reconnection, but not in unipolar regions. The consequence of the annihilation of subdominant flux is a sharp reduction in the number of sectors and a loss in magnetic flux, as documented from the *Voyager 1* magnetic field and flow data.

Key words: magnetic reconnection – Sun: heliosphere – Sun: magnetic fields

Supporting material: animation

1. Introduction

The rotation of the Sun twists the solar dipole field into the dominant azimuthal Parker spiral magnetic field B_T separated by the heliospheric current sheet. Because of the misalignment of the solar rotation axis and magnetic axis, the current sheet flaps in the vertical direction as it propagates outward from the Sun, producing the sectored magnetic field (Wilcox & Ness 1965) in which the azimuthal magnetic field B_T reverses sign about every 13 days (the RTN coordinate system is defined with R in the radial direction, T in the azimuthal direction with positive T in the direction of the Sun's rotation, and N, which points north in the equatorial plane, completes the triad). The sector zone occupies a latitudinal extent that varies during the solar cycle; it nearly reaches the poles when the fields from the Sun are at maximum (Smith 2001).

An important question is whether the sectored magnetic field can reconnect to release magnetic energy and accelerate particles. In the solar wind around 1 au, the heliospheric current only occasionally undergoes reconnection (Gosling 2007), probably because the current sheet is far wider than the characteristic ion inertial scale $d_i = c/\omega_{pi}$ (where collisionless reconnection sets in) (Cassak et al. 2005). As a result, the sector stucture of the solar magnetic field survives out to the termination shock (TS) even though the periodicity of the current sheet becomes increasingly irregular with distance from the Sun (Burlaga et al. 2003, 2005, 2006). It has been suggested that the drop in the solar wind density with distance and therefore the increase in d_i, combined with the compression of the current sheets downstream of the TS, leads to the onset of reconnection in the sectored heliosheath (HS). This reconnection has been proposed as a source of free energy to drive the production of anomalous cosmic rays (ACRs) (Drake et al. 2010; Opher et al. 2011) and as a source of turbulence in the heliosheath that might control the transport of energetic particles (Burgess et al. 2016). The reduction of the plasma flow in the HS on its approach to the heliospause is expected to further compress the sectored magnetic field, inevitably leading to the onset of reconnection in the HS (Czechowski et al. 2010; Drake et al. 2010; Borovikov et al. 2011; Opher et al. 2011). However, determining the thickness of the heliospheric current sheets downstream of the TS to confirm that collisionless reconnection should onset in the HS is a challenge because of the low and variable speed of plasma flows in the HS and because weak magnetic fields there are difficult to measure. It has been suggested that current sheets in the HS are thicker than the ion inertial scale (Burlaga & Ness 2011), but post-reconnection final states are characterized by magnetic islands in which current layers are comparable in width to the island width. Thick current sheets might therefore suggest that reconnection in HS has already taken place.

In any case, compelling evidence from the *Voyager* observations that reconnection in the sectored HS has taken place has not been identified. The challenge is that the *Voyager* magnetometers were not designed to measure the weak magnetic fields in the outer heliosphere (~0.1 nT with noise levels ~0.05 nT) and *Voyager 1* has no plasma measurements. Furthermore, the dynamics of reconnection in the high β

environment of the HS remains relatively poorly understood (Schoeffler et al. 2011, 2013) compared with the typically $\beta \sim 1$ conditions at 1 au. The multiple sharp dropouts of energetic particles of heliospheric origin measured by *Voyager 1* at the HP boundary (Stone et al. 2013) do suggest the existence of magnetic islands and therefore magnetic reconnection at and in the vicinity of the HP (Strumik et al. 2013, 2014; Swisdak et al. 2013).

There are a variety of indirect indicators that reconnection is active in the HS, including the loss in magnetic flux documented by *Voyager 1* (Richardson et al. 2013) and the dropouts in the low-energy electrons at *Voyager 2* (Opher et al. 2011; Hill et al. 2014). In the absence of reconnection, the azimuthal magnetic flux $V_R R B_T$ is preserved in the heliosphere in regions where the flow is dominantly radial. While *Voyager 1* was in the HS, the radial flow V_R dropped essentially to zero (Krimigis et al. 2011), while there was no significant increase in B_T. A significant flow in the N direction (to the north in the case of *Voyager 1*) might convect the flux away and therefore prevent the pileup of B_T. However, the *Voyager 1* data suggested that V_N was also very small (Decker et al. 2012; Stone & Cummings 2012). It therefore seems likely that reconnection must be playing a role in the *Voyager 1* flux loss measurements. On the other hand, reconnection does not normally reduce the magnetic flux in a reconnecting current layer. Rather, the flux that reconnects at an x-line is convected into the adjacent magnetic island such that the integrated magnetic flux is preserved (Fermo et al. 2010). The flux loss issue can therefore not be simply be resolved by invoking reconnection without a more careful analysis. The dropouts in low-energy electrons at *Voyager 2* were attributed to *Voyager 2* leaving the sector zone (Opher et al. 2011; Hill et al. 2014). The argument was that electrons can rapidly escape from a region of the heliosheath with laminar (unreconnected) magnetic fields, while reconnected magnetic fields and associated magnetic islands would be more effective in suppressing electron transport along the ambient magnetic field. Thus, higher electron fluxes in the sectored heliosheath are evidence that the heliosheath magnetic field had reconnected—in the absence of reconnection, there is no reason that the transport properties of the sectored and non-sectored HS should differ.

The *Voyager* observations in the HS have uncovered other issues related to the reconnection or lack thereof of the sectored magnetic field. The first concerns the polarity of the HS magnetic field. The nominal polarity of the magnetic field in the northern hemisphere during the time period 2000–2011 is negative (corresponding to the azimuthal angle $\lambda = \arctan(B_T/B_R) = 90^\circ$) (Burlaga & Ness 2012; Richardson et al. 2016). When *Voyager 1* is in the sector zone, λ typically flips back and forth between 90° and 270°, and a long period of 90°, which occurred in 2011, would normally be interpreted as an excursion beyond the sector zone and into the unipolar zone. On the other hand, the magnetohydrodynamic (MHD) models of the global heliosphere predict that the sector zone should be convected to the north as the HS plasma approaches the HP so that *Voyager 1* should remain within that sector zone before its crossing of the HP (Borovikov et al. 2011; Opher et al. 2011). Similarly, in 2011–2012, *Voyager 2* saw significantly fewer excursions into negative (northern latitude polarity) than expected based on the Wilcox Solar Observatory predictions (Richardson et al. 2016). Why the *Voyagers* are seeing fewer excursions into magnetic field polarities that are opposite to their heliolatitude is a mystery.

A second mystery concerns the distinct magnetic structures seen in the *Voyager 1* and *2* data. At proton boundary layers (PBLs), the magnetic field strength either rises or drops by factors of up to three with no measureable change in the azimuthal angle λ or the elevation angle $\delta = \arcsin(B_N/B)$ (the angle of the magnetic field with respect to the R–T plane) (Burlaga & Ness 2011, 2012). Since these regions of magnetic field enhancement or depletion can last for days, it seems unlikely that they are associated with kinetic scale instabilities such as mirror modes, which typically produce localized humps in the magnetic field rather than depletions in high β plasma (Baumgärtel et al. 2003).

Here we address the dynamics of reconnection in the sectored HS with the goal of understanding the signatures and consequences of the reconnection and the resultant structure of the HS magnetic field. The simulations extend earlier models by considering more realistic initial conditions that account for unequal positive and negative azimuthal magnetic flux. That the sector zone does not carry equal postive and negative flux at the latitudes of the *Voyager* spacecraft trajectories is evident from the *Voyager* observations in the solar wind in the outer heliosphere, but upstream of the TS (Burlaga et al. 2003). In this region, because the solar wind velocity greatly exceeds the spacecraft velocity, time in a region of given polarity is linked to the integrated magnetic flux in a given sector. The *Voyager* data in the high-speed solar wind of the outer heliosphere reveals that sector spacing is highly erratic, and therefore positive and negative fluxes are unequal. For the time period 2000–2011, one might expect that for *Voyager 1* the negative polarity dominates because the spacecraft was closer to the northern boundary of the sector zone, which has negative polarity, while for *Voyager 2* positive polarity dominates. Unequal magnetic fluxes were required to reproduce *Voyager 1* magnetic data in MHD simulations of reconnection at the HP (Strumik et al. 2014).

The consequence of unequal fluxes is profound. At late time, when reconnection is nearly complete, bands of single polarity flux survive, which tends to organize the sector structure more than in earlier simulations in which magnetic islands dominated the magnetic structure at late time (Drake et al. 2010; Opher et al. 2011). The simulations are also carried out with high initial β and with initial force-free current layers rather than Harris-type current layers, which are typically not seen even at 1 au (Smith 2001). Because of the high β, the magnetic field at late time exhibits large-scale depletions in which the magnetic field strength drops by around a factor of three over a narrow boundary layer with little variation in the direction of the magnetic field. The plasma density and temperature rise slightly within the depletions to maintain pressure balance. The radial width of these magnetic depletions is around three times the width of the initial sector with the subdominant magnetic flux. The depth of these depletions and their widths (when normalized to the initial separation of current layers) are universal values that are linked to the intrinsic properties of collisionless magnetic reconnection. The boundaries of these magnetic depletions exhibit a striking resemblance to the PBLs seen in the *Voyager* data. We show that reconnection on adjacent current layers conspires to completely annihilate the subdominant magnetic flux, leading to regions of unipolar flux. Pairs of magnetic islands do survive at late time, although the

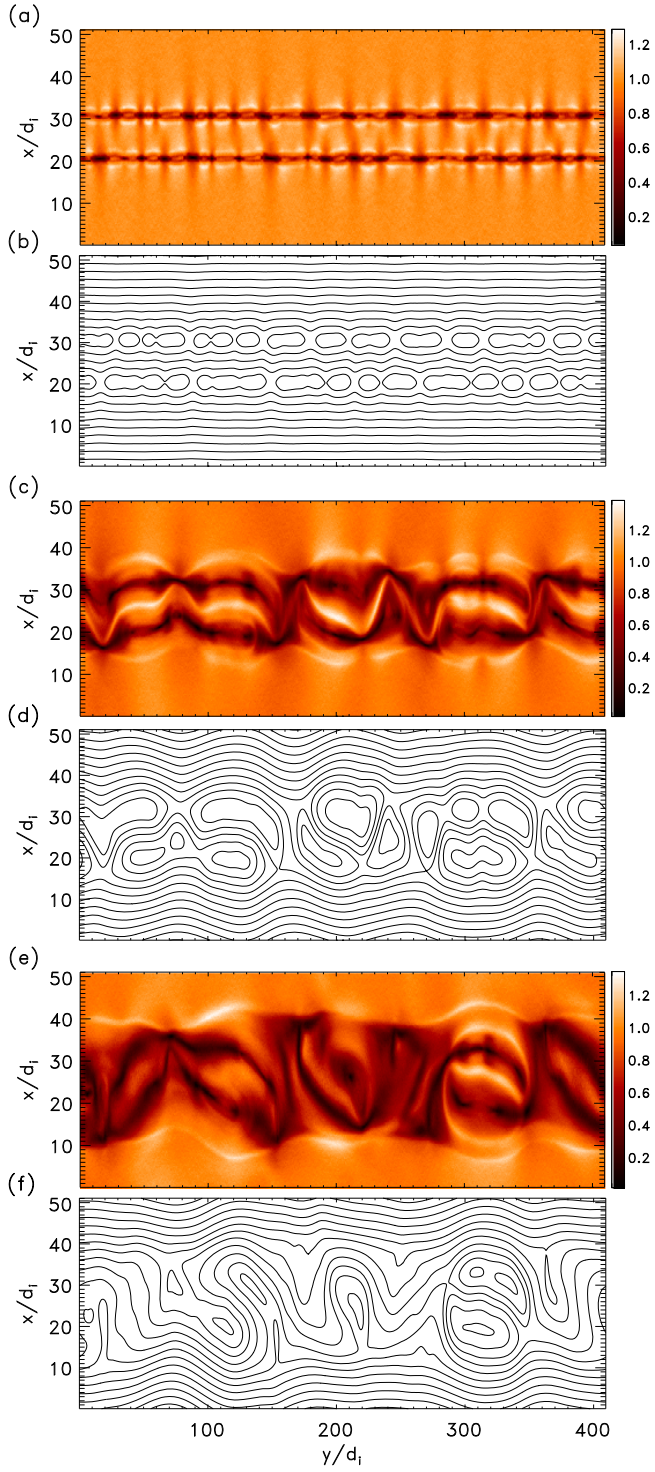

Figure 1. The magnetic structure in the lower half of the simulation domain at $\Omega_i t = 50$, 200, and 350 during the simulation. The magnetic field B is shown in (a), (c), and (e), and the in-plane field lines are shown in (b), (d), and (f). The magnetic field B from the simulation is available online as a video figure. The video runs from time zero to $\Omega_i t = 440$. and shows the actual aspect ratio of the lower half of the computational domain.

(An animation of this figure is available.)

volume of plasma associated with these remnant islands is small compared with the regions of magnetic depletion. The island structures exhibit magnetic dips and rotations in the magnetic field direction that might be interpreted as sector crossings in satellite data. The simulations therefore offer a possible explanation of the predominance of unipolar flux and the loss of magnetic flux seen in the *Voyager 1* magnetic field data. Finally, analysis of the *Voyager 2* magnetic field and plasma data reveals that fluctuations in magnetic field strength and density are anticorrelated in the sectored HS, as expected from reconnection, but not in the unipolar HS. As a whole, the consistency of the *Voyager* data with unique reconnection signatures establishes with high likelihood that reconnection in the sectored HS has taken place.

2. Particle-in-cell (PIC) Model and Initial Conditions

We carry out 2D particle-in-cell (PIC) simulations of the sector structure in the $x - y$ plane of the simulation, which maps to the heliospheric $R - T$ plane. The simulations are performed with the PIC code p3d (Zeiler et al. 2002) using a periodic equilibrium magnetic field

$$\frac{B_y}{B_0} = \tanh\left(\frac{x - 0.2L_x}{w_0}\right) - \tanh\left(\frac{x - 0.3L_x}{w_0}\right) + \tanh\left(\frac{x - 0.7L_x}{w_0}\right) - \tanh\left(\frac{x - 0.8L_x}{w_0}\right) - 1. \quad (1)$$

For this magnetic configuration there are four current layers centered at $x/d_i = 20.48$, 30.72, 70.68, and 81.92 on a computational domain that is $L_y \times L_x = 409.6 \times 102.4$, where lengths are expressed in units of $d_i = c_A/\Omega_i$, the proton inertial length. The total magnetic flux in the negative y direction is four times that in the positive y direction. The initial plasma density n_0 and temperatures T_e and T_i are constants, and the out-of-plane magnetic field $B_z^2 = B_0^2 - B_y^2$ is chosen to produce force balance. This initial state is not a rigorous kinetic equilibrium, especially for ions, but does not display unusual behavior at early time. The results are presented in normalized units: the magnetic field to the asymptotic value of the reversed field B_0, the density to n_0, velocities to the proton Alfvén speed $c_A = B_0/\sqrt{4\pi m_i n_0}$, times to the inverse proton cyclotron frequency, $\Omega_i^{-1} = m_i c/eB_0$, and temperatures to $m_i c_A^2$. We define some additional scale lengths as follows: $w_0 = 0.25d_i$ is the half-width of an individual current sheet, and $\Delta_x = \Delta_y = 0.05d_i$ are the grid scales. To maximize the separation between the macroscales L_x and L_y and the kinetic scales, we choose a modest ion-to-electron mass ratio of 25 and velocity of light c of $15c_A$. The particle temperatures are initially uniform with $T_i = 5.0m_i c_A^2$ and $T_e = 2.0m_i c_A^2$, so that $\beta = 8\pi n_0(T_e + T_i)/B_0^2 = 14$ is large, as expected for the heliosheath. The average number of particles per cell is 100. Reconnection begins from particle noise.

The overall scale sizes of our simulations are much smaller than those of the heliospheric sectored field. The widths of the sectors upstream of the TS are around 1.7×10^8 km, which at a density of $0.001/\mathrm{cm}^3$ is around $2 \times 10^4 d_i$. Compression across the shock and the approach to the heliopause reduces the sector width somewhat, but the sector spacing continues to be far larger in units of d_i than the values we can implement in our simulations. However, we have shown earlier that the growth rate of islands is insensitive to the kinetic scale d_i (Schoeffler et al. 2012), and the same conclusion applies to the simulations presented here. Thus, the reconnection rates and associated bulk ion flows can be translated into the heliosheath by

normalizing to the Alfvén speed and the Alfvén transit time L_x/c_A.

3. Simulation Results

In Figure 1 we show 2D plots of the magnetic field strength B and the magnetic field lines around the two lower current layers in the system at times $\Omega_i t = 50$, 200, and 350. The initial magnetic field points to the left above and below the two current layers and to the right between the two layers. In (a) and (b), a large number of very small islands grow on the two current layers at early time. These islands coalesce and continue to grow, until in (c) and (d) they span the entire region between the adjacent current layers. At this point, all of the magnetic field lines spanning the simulation domain in the positive y direction have reconnected. On the other hand, positive magnetic flux still exists. Along a single cut in x in (d), B_y has positive and negative values. However, island merging and reconnection continues, and at later time in (e) and (f), much of the positive magnetic flux has been annihilated. How this happens is important first because of the flux loss documented by the *Voyager 1* observations and second because magnetic reconnection normally preserves the magnetic flux. At the magnetic x-line, field lines reconnect, but the integrated unsigned flux through a magnetic island is unchanged as reconnection proceeds. Namely, there is no flux loss at the center of the island, and magnetic flux is preserved elsewhere so that the total magnetic flux contained in an island is preserved. On the other hand, it is evident from Figure 1(f) that on a cut along x at $y \sim 240$, B_y will only have negative values —there is no surviving positive flux in this region.

The pressure anisotropy that develops during magnetic reconnection in a high β system such as the HS weakens the tension force exerted by the magnetic field on the plasma and therefore slows reconnection and allows islands to take elongated forms (Drake et al. 2010; Opher et al. 2011; Schoeffler et al. 2011). A video animation of the magnetic field B for the full duration of the simulation domain (up until $\Omega_{ci} t = 440$.) is available in an online animated version of Figure 1. The movie reveals that the evolution of the magnetic field slows dramatically at late time, a consequence of the pressure anisotropy, and allows isolated elongated magnetic islands to survive late in time.

In Figure 2 we show a blowup of B and associated magnetic field lines at four times to illustrate how flux anniliation in the geometry of the sectored heliosphere takes place. Again, the magnetic field lines above and below the two current layers initially point to the left, and between the two current layers, they point to the right. In (a) magnetic islands on the two current layers do not yet cross-connect with the adjacent current layer, and there is positive magnetic flux that spans the domain in y. In (b) the magnetic separatrix of the large island on the lower current layer connects with the upper current layer. At this point, there is still substantial positive magnetic flux even though there are no positive B_y field lines that span the system along the y direction. However, the positive magnetic field B_y of the island on the lower current layer begins reconnecting with the negative flux above the upper current layer, which annihilates the positive flux. In (d) almost all of the magnetic flux in the island from the lower current layer has been annihilated, eliminating the surviving positive flux.

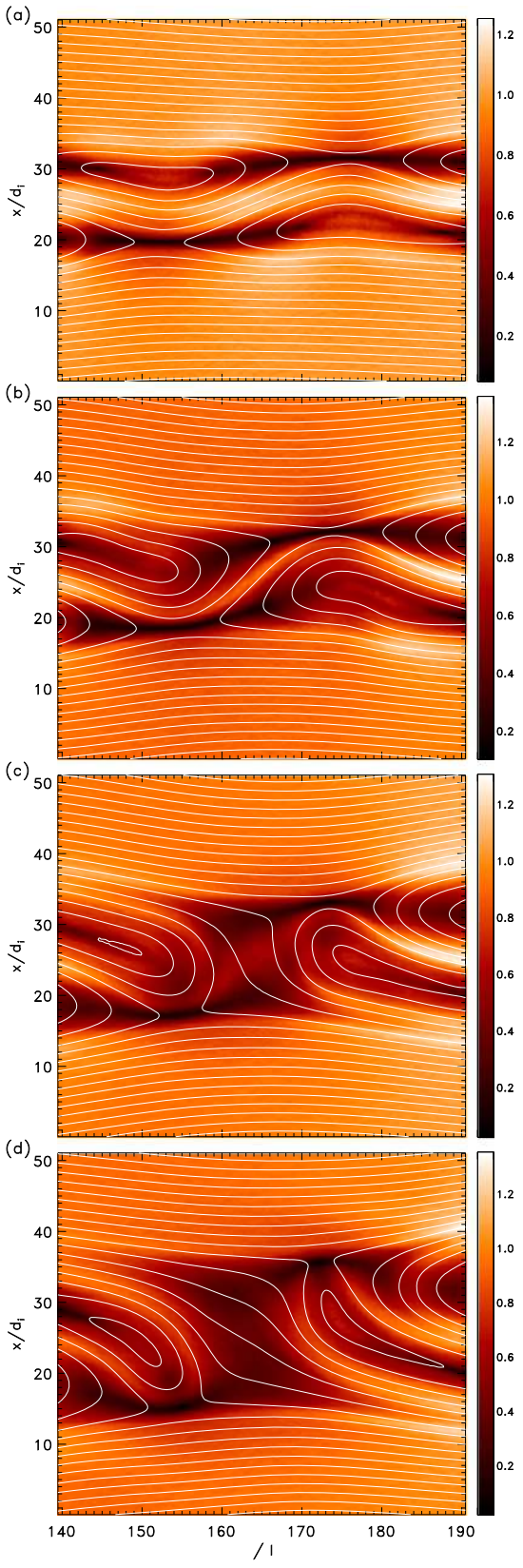

Figure 2. A blowup view of the time evolution of a pair of magnetic islands at $\Omega_i t = 100$, 150, 200, and 250 showing how the subdominant flux is annihilated. The magnetic field B is shown in color and the overlaid white lines are magnetic field lines. The times shown are before the islands overlap the adjacent current layer in (a), when they first intersect the adjacent current layer in (b), and when the magnetic flux in the islands is eroded in (c) and (d).

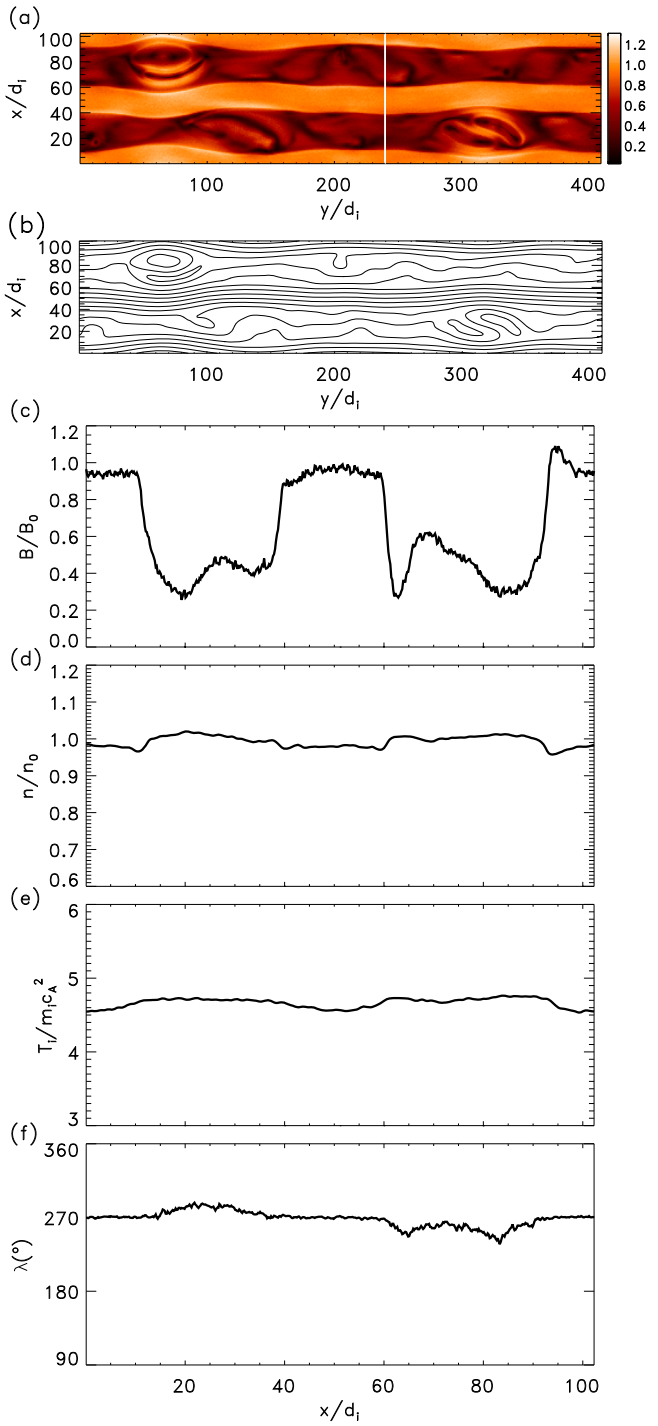

Figure 3. The late-time ($\Omega_i t = 440$) structure of the magnetic field B in (a) and magnetic field lines in (b) over the entire simulation domain. Cuts across the magnetic depletions along the white line in (a) showing B in (c), of the density n in (d), the ion temperature T_i in (e), and the azimuthal angle λ in (f).

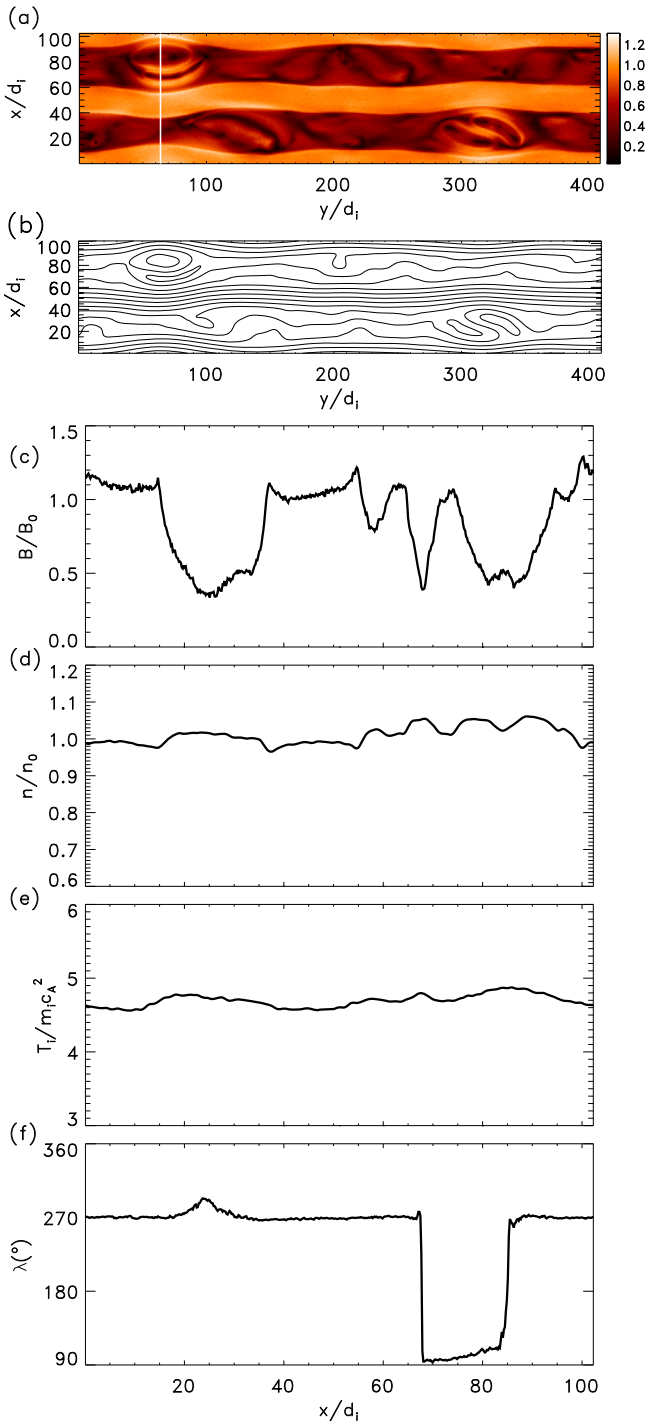

Figure 4. The late-time ($\Omega_i t = 440$) structure of the magnetic field B in (a) and magnetic field lines in (b) over the entire simulation domain. Cuts through a remnant pair of magnetic islands along the white line in (a) showing B in (c), of the density n in (d), the ion temperature T_i in (e), and the azimuthal angle λ in (f).

The late-time ($\Omega_p t = 440$) structure of the magnetic fields, density, and temperature of the full simulation domain are shown in Figures 3 and 4. In Figures 3(a) and (b) we show B and field lines of the entire $x - y$ computational domain. Surviving at late time are two pairs of islands embedded in a lower and upper band of depleted magnetic energy. Elsewhere, the islands have reconnected away, leaving only negative magnetic flux. The structure of the magnetic depletions is futher illustrated in cuts of B in (c), n in (d), T_i in (e), and the azimuthal angle $\lambda = \arctan(B_y/B_x)$ in (f), where λ defines the direction of the magnetic field in the $x - y$ plane with respect to the x direction. The location of the cut is marked by the white line in Figure 3(a). The cut in Figure 3(a) is chosen specifically because it represents what a satellite might typically see in a heliosheath where reconnection has already annihilated significant magnetic flux. The strong depletions of the magnetic field seen in (c) span the region around each pair

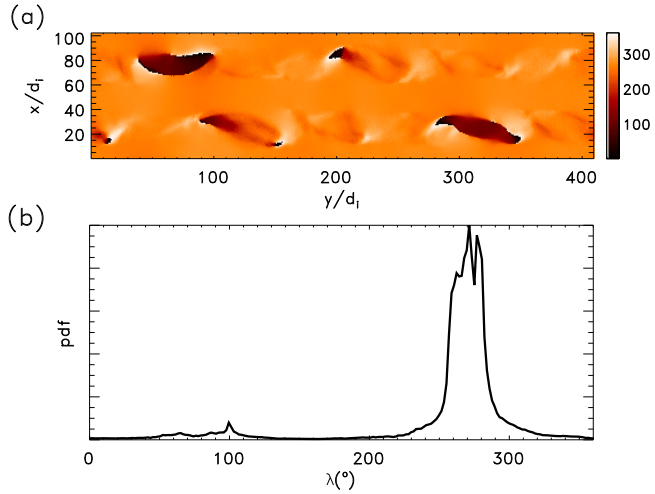

Figure 5. At late time, the spatial distribution of the azimuthal angle λ in the full simulation domain (a) and its probability distribution in (b). Note the prominence of the dominant magnetic polarity at late time. The ratio probability of dominant to subdominant polarity in the initial state was four.

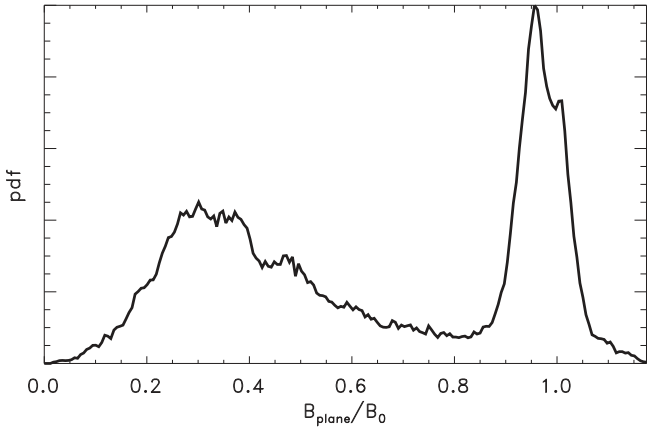

Figure 6. From the simulation at late time, the probability distribution function (pdf) of the strength of the in-plane magnetic field $B_{\rm plane} = \sqrt{B_x^2 + B_y^2}$. Note the distinct peak at $B_0/3$.

of adjacent current layers in the initial system and are a consequence of growth and merger of magnetic islands on adjacent current layers. The boundaries of the magnetic depletions mark the maximum spatial extent of reconnection of adjacent current layers. Pressure balance is maintained within the magnetic depletions by small increases in the density and ion temperature. The increase in electron temperature (not shown) is even smaller. In the cut shown here, the azimuthal angle λ is nearly constant at 270°. In this region, all of the initial positive flux has been annihilated. The scale length of the boundaries of the magnetic depletions are expected to scale with the proton Larmor radius ρ_i because the protons carry most of the pressure, and they are able to decouple from the magnetic field on scale lengths of the order of several ρ_i (Drake et al. 2009). For the simulation of Figure 3, the proton Larmor radius is around $2.2d_i$, so that the scale lengths of the boundaries of the magnetic depletions in Figure 3(c) are 3–5ρ_i. We emphasize that the scale lengths of these boundary layers are insensitive to the initial width of the initial current sheets because the boundaries are associated with the upstream edges of the reconnection exhaust, which is controlled by local physics—ions move from upstream into the exhaust and are accelerated up to the Alfvén speed across a narrow boundary layer (Drake et al. 2009).

Figure 4 is similar to Figure 3, but the cuts are now taken through the pair of magnetic islands on the top band of the depleted magnetic field. Again, the white line shows the location of the cut in Figure 4(a). The centers of the two islands can be seen in Figure 4(b), but are most evident in the cut of λ, which jumps sharply from 270° to 90° and back across the centers of the islands. The island centers are locations of minima of B and small peaks in the density and ion temperature. Distinguishing the crossing of such an island from the crossing of the heliospheric current sheet in the heliosheath would be difficult because the traditional signatures of reconnection, such as high-speed flow, have died away—the system has evolved to a quasistatic state. We emphasize that the probability of crossing a region where the subdominant magnetic flux survives at late time in the system is small. In Figure 5 the spatial distribution of λ at late time is shown in (a), and in (b) we show the probability distribution of λ. The probability of finding $\lambda \sim 90°$ in this simulation at late time is finite but small.

We can give estimates for the widths and size of the magnetic depletions based on how reconnection developed to produce the final states shown in Figures 3 and 4. The total width of the magnetic depletion can be calculated by determining the spatial extent of reconnection leading to the final state. Consider two adjacent current layers separated by a distance δL with a total magnetic flux between the two layers $\delta\psi$. The separatrix magnetic field line that connects to the two x-lines in Figure 2(b) was originally at the center of the region between the two nearby current layers at $x/d_i = 20$ and 30. Thus, during the reconnection that led to this state, half of the magnetic flux in the region between the two current $\delta\psi$ layers reconnected with the flux above the current layer at 30 and half reconnected with the flux below the current layer at 20. Thus, the spatial extent in x of the entire region inside of the reconnected field lines is $2\delta L$ ($\delta L/2$ above the upper current layer, $\delta L/2$ below the lower current layer, and the region δL between the two current layers). During the time from Figure 2(b) to late time, the remaining positive flux $\delta\psi/2$ surrounding the island centered at $x \sim 20$ and $y \sim 185$ reconnects with the negative flux above the upper current layer. At the end of this reconnection process, the island is gone. The same happens as the positive flux in the island centered at $x \sim 30$ and $y \sim 145$ reconnects with the negative flux below the lower current layer. The reconnection of these two islands with flux above and below extends the reconnection zone another distance $\delta L/2$ above and below the reconnection zone shown in Figure 2(b). Thus, at the end of the reconnection process, the total extension of the reconnection zone is $3\delta L$. The total surviving magnetic flux over this domain is $\delta\psi$ ($\delta\psi$ each from above and below the initial current layers and $-\delta\psi$ from between the current layers). Since this flux is spread out over a distance that is three times the initial separation of the current layers, the magnetic field strength is $B_0/3$, independent of the size of the simulation domain, current layer separation, or plasma parameters. The cuts of B in Figure 3(c) display depletions with widths that are around 30, consistent with this estimate, and with magnetic field minima that are close to $0.33B_0$. A probability distribution function (pdf) of the magnitude of the in-plane magnetic field $B_{\rm plane}$ is presented in Figure 6. There are distinct peaks in the pdf at the

initial magnetic field strength B_0 and at $B_0/3$. Of course, if the disparity between positive and negative flux is insufficient, the magnetic islands growing on all current layers will ultimately overlap and the organized magnetic depletions shown in Figures 3 and 4 will not characterize the final state. The disparity between positive and negative flux needs to exceed two for the isolated depletions to survive at late time.

4. Observational Results from *Voyager 2*

Our simulations of the sectored HS suggest that large depletions in the magnetic field result from magnetic reconnection. The PBLs (Burlaga & Ness 2011, 2012) that have been identified in the *Voyager 1* and *2* data look very much like the boundaries of the strong magnetic depletions that we see in our simulations. Because reconnection-driven flows are Alfvénic and therefore fall below the local magnetosonic velocity in the high-β heliosheath, reconnection dynamics is to lowest order incompressible, which means that depletions in the magnetic field pressure correspond to enhancements in the plasma density and pressure. This can be seen in the cuts across the magnetic depletions in the simulation data presented in Figures 3 and 4. Thus, if the magnetic field disturbances in the sectored heliosheath are driven by reconnection, they should correspond to perturbations in the density such that deviations of the magnetic field, and density from the ambient background are anticorrelated—reductions (increases) of the magnetic strength should correspond to local increases (decreases) in the plasma density. In the non-sectored heliosheath this anticorrelation should not be present unless there are mechanisms for generating non-compressible turbulence other than reconnection.

Thus, we have explored the correlation between magnetic field and density fluctuations in the *Voyager 2* data sets. The plasma instrument on *Voyager 1* failed many years ago, so correlation studies with the *Voyager 1* data are not possible. We have compared the fluctuations of the density (dn) and magnetic field magnitude (dB) in a heliosheath region where the sector structure is observed (2008.2–2009.15, 344 days of data) with those in a unipolar region (2009.15–2010.5, 455 days of data) (Burlaga & Ness 2011; Richardson et al. 2016). We use daily averages of the magnetic field magnitudes from the SPDF website and of the density from the MIT *Voyager* website. Figure 7 shows histograms of $\langle dBdn\rangle \Big/ \sqrt{\langle dB^2\rangle \langle dn^2\rangle}$ where $dB = B - \langle B\rangle$ and $dn = n - \langle n\rangle$. The average $\langle A\rangle$ of any quantity A is defined over a 25-day averaging window. The histograms are clearly different for the two regions, with dB and dn usually having opposite signs (anticorrelated) in the sector region, but not in the unipolar region. Thus, the *Voyager 2* data suggest that fluctuations in the sectored heliosheath are driven by reconnection. Alternative explanations for the anticorrelation between the fluctuations in the magnetic field intensity and density would need to explain why the fluctuations are anticorrelated in the sectored zone, but not in the unipolar region.

To compare this correlation data with data from our simulation, we evaluate

$$\frac{\delta n \delta B_{\rm plane}}{\sqrt{\langle \delta n^2\rangle \langle \delta B_{\rm plane}^2\rangle}}$$

with $\delta f = f - \langle f\rangle$ for any function f and where $\langle f\rangle$ is an average over the simulation domain. The pdf of this function is shown in Figure 8. As in the observational data, the perturbations of the density and $B_{\rm plane}$ are anticorrelated since there is a distinct shift in the data toward negative values. The average of this pdf data is the correlation function of δn and $\delta B_{\rm plane}$. It has a value of -0.73.

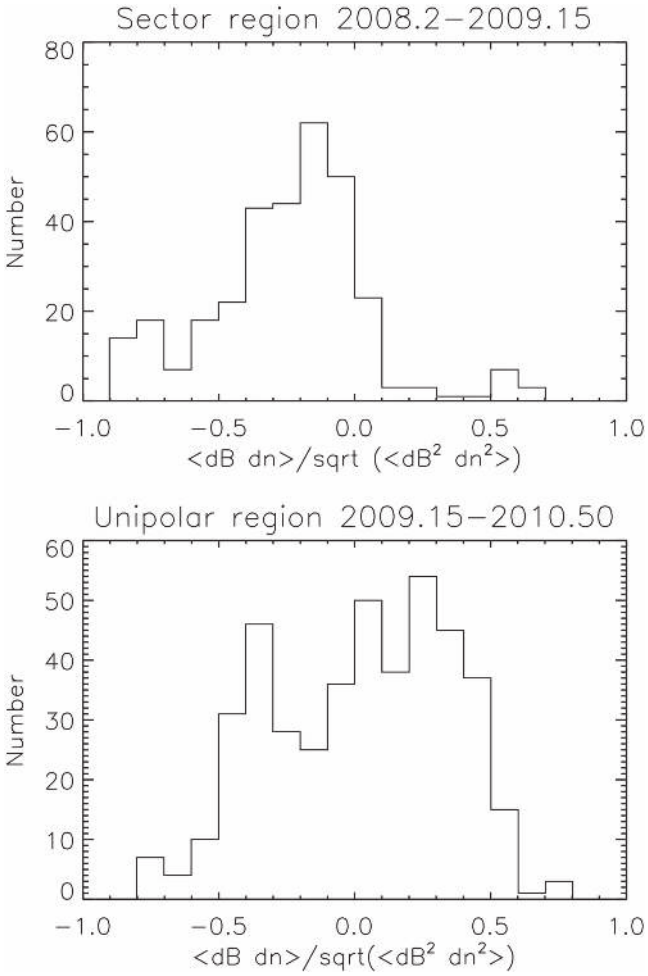

Figure 7. Histograms of $\langle dBdn\rangle \Big/ \sqrt{\langle dB^2\rangle \langle dn^2\rangle}$ where $dB = B - \langle B\rangle$ and $dn = n - \langle n\rangle$ from *Voyager 2* in the sectored region (top) and the unipolar region (bottom). We use 25-day averaging windows.

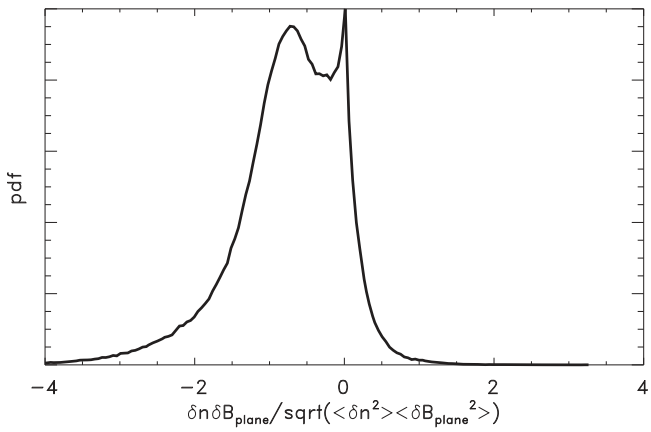

Figure 8. From the simulation a histogram of $\delta n \delta B_{\rm plane} \Big/ \sqrt{\langle \delta B_{\rm plane}^2\rangle \langle \delta n^2\rangle}$, where $\delta n = n - \langle n\rangle$, $\delta B_{\rm plane} = B_{\rm plane} - \langle B_{\rm plane}\rangle$ with n the density, $B_{\rm plane}$ the magnitude of the in-plane magnetic field, and $\langle n\rangle$ and $\langle B_{\rm plane}\rangle$ the average over the computational domain.

5. Discussion

We have carried out kinetic simulations of magnetic reconnection in the sectored heliosheath that include the asymmetry in the magnetic flux in the sectors that is expected near the northern and southern latitude boundaries of the heliospheric sector zone. We show that when the magnetic flux asymmetry is more than a factor of two, bands of unreconnected magnetic flux B_T survive and sandwich bands that have a strongly depleted magnetic field. In the final state, the widths of the depletion regions are around three times the width of the initial current layer separations, with magnetic field strengths that are around one third of the pre-reconnection intensity. The boundaries of the depletion regions are sharp—several times the proton Larmor radius. The reconnection of magnetic islands on adjacent current sheets leads to the nearly complete annihilation of flux in the subdominant direction. This flux annihilation does not typically take place during magnetic island growth on a single current layer because magnetic islands conserve the integrated magnetic flux. The final state has scattered pairs of remnant magnetic islands in which the subdominant magnetic flux survives. Cuts across these islands would appear like crossings of an undisturbed heliospheric current sheet—the azimuthal angle λ jumps sharply from 90° to 270° and then reverses across the cores of these islands (Figure 4). The probability of crossing such an island, however, is low compared to that of crossing a pristine region of magnetic depletion (Figure 3).

In the spherically expanding solar wind, the conservation of magnetic flux implies that $V_R B_T R$ is a constant. For a constant solar velocity V_R, this expression yields the usual falloff of B_T as $1/R$, which has been documented in the solar wind. In the heliosheath the magnetic field is more complex because of the development of latitudinal flows V_N. However, it was a major surprise when the estimated radial plasma flows V_R at the *Voyager 1* spacecraft dropped to essentially zero in 2010 (Krimigis et al. 2011) and yet the magnetic field strength did not increase to compensate (Burlaga & Ness 2012). Since the velocity V_N was also close to zero, the loss of magnetic flux through a flow to high latitude was insufficient to explain the apparent loss of flux. The conclusion therefore was that the *Voyager 1* observations documented a flux loss in the heliosheath (Richardson et al. 2013). In contrast, the magnetic field and flow measurements at *Voyager 2* suggested that flux was conserved along its trajectory.

The model presented here might explain how magnetic flux could be lost in the sectored heliosheath. Of course, if flux annihilation as discussed here did take place in the heliosheath at the location of *Voyager 1*, one would expect to see fewer sector crossings than expected in the magnetic field data. From 2010 to the heliopause crossing in mid-2012, the *Voyager 1* spacecraft did see less southern polarity flux than expected from the WSO data. However, during the long period during which the measured value of V_R decreased at *Voyager 1*, the data do not suggest a reduced probability of southern polarity magnetic flux. Indeed, there is an unexplained period during 2008–2010 when the probability of seeing southern polarity flux is much higher than expected (Richardson et al. 2016). Magnetic reconnection nevertheless seems to be the only viable mechanism that can explain the flux loss along the *Voyager 1* trajectory.

The challenge is to identify a more direct method of establishing whether reconnection is taking place in the heliosheath. This is not easy because crossing a current sheet where reconnection is actually taking place is highly improbable. There have now been several hundred identifications of active reconnection in the solar wind at 1 au, and yet there is not a single documented observation of the crossing of a magnetic x-line where active reconnection is ongoing—how does one distinguish a static current layer from a current layer where reconnection is active? This requires the accurate measurement of the intense Hall electric field that bounds the current layer on either side of the x-line (Drake et al. 2008), which has not been measured in the solar wind. The documented reconnection observations (Gosling et al. 2005; Gosling 2007) are crossings of the reconnection exhaust, where the measured exhaust velocity has been cross-checked with the predictions based on the Walén condition (Hudson 1970). What are the corresponding direct signatures of reconnection in the heliosheath? We have argued previously that if reconnection sets in just downstream of the TS, where the heliospheric current sheet should be compressed below the ion inertial scale d_i, the growth time for islands to reach the characterisic sector spacing should be around 60 days, which translates into a distance around 2–3 au downstream of the TS (Schoeffler et al. 2012). Deep within the heliosheath, the sectors should therefore have reconnected and the signatures of reconnection should be reflected in the late-time structure of the magnetic remnants of reconnection rather than an active reconnection site. That reconnection is taking place in the heliosheath is also supported by the ACR spectra, which peak well downstream of the TS (Decker et al. 2005, 2008; Stone et al. 2005). Reconnection downstream of the TS is one possible explanation of these observations (Drake et al. 2010; Opher et al. 2011). Some more recent theoretical models suggest that reconnection dynamics downstream of the shock is an intrinsic component of the TS structure and associated particle acceleration (Zank et al. 2015).

In the core of the sector zone, where the positive and negative polarity fluxes are nearly equal, the late-time state consists of elongated magnetic islands (Opher et al. 2011), while closer to the latitudinal boundaries of the sector zone, where positive and negative polarity fluxes are not equal, the spacecraft observations should resemble the cuts shown in Figures 3 and 4. The magnetic depletions across rather narrow boundary layers, which can extend to several astronomical unit in width, are the clearest direct signatures of the post-reconnection heliosheath. The PBLs that have been documented in the *Voyager 1* (Burlaga & Ness 2011, 2012) and 2 (Burlaga et al. 2016) data are very similar to the magnetic depletions that appear in our simulations. A surprise is that many of the clearest examples of PBLs from the *Voyager 1* data seem to have jumps in magnetic field strength that are around three, which is the value that follows from our analysis of the reconnection dynamics. The measured scale lengths of the measured PBLs are $5–10\rho_i$, which are modestly wider than those seen in our simulations. Other suggestions are that the PBLs result from the growth of mirror modes (Burlaga & Ness 2011, 2012). However, mirror modes tend to take the form of humps rather than depletions in high β systems (Baumgärtel et al. 2003), and the overall spatial scale of the depletions from mirror modes is far smaller than the typical depletions measured in the heliosheath. In contrast, the size of the depletions from reconnection are not linked to any kinetic scale but to the radial scale length of the sectors, which can be

of the order of an astronomical unit. The depletions from mirror modes would also require a significant magnetic field component in the N direction so that the elevation angle δ would be substantial. High values of δ that extend over the regions of magnetic field depletion are not typically seen in the spacecraft data.

Finally, intrinsic to reconnection in a high-β system such as the HS, where the Alfvén speed is well below the magnetosonic speed, is that the dynamics is nearly incompressible so that the magnetic depletions seen in the simulations are supported by corresponding increases in the plasma pressure (and density). Thus, the fluctuations in the magnetic field strength and density from reconnection should be anticorrelated. The data from *Voyager 2* confirm the anticorrelation of fluctuations in magnetic field strength and density in the sectored HS, but not in the unipolar HS, as expected if reconnection is taking place in the sectored HS.

This work has been supported by NASA Grand Challenge NNX14AIB0G, NASA awards NNX14AF42G, NNX13AE04G, and NNX13AE04G, and NASA contract 959203 from JPL to MIT. The simulations were performed at the National Energy Research Scientific Computing Center. We acknowledge fruitful discussions with Dr. Len Burlaga on the *Voyager* observations and with Dr. Obioma Ohia on outer heliosphere reconnection. This research benefited greatly from discussions held at the meetings of the Heliopause International Team Facing the Most Pressing Challenges to Our Understanding of the Heliosheath and its Outer Boundaries at the International Space Science Institute in Bern, Switzerland.

References

Baumgärtel, K., Sauer, K., & Dubinin, E. 2003, GeoRL, 30, 1761
Borovikov, S. N., Pogorelov, N. V., Burlaga, L. F., & Richardson, J. D. 2011, ApJL, 728, 21
Burgess, D., Gingell, P. W., & Matteini, L. 2016, ApJ, 822, 38
Burlaga, L. F., & Ness, N. F. 2011, JGRA, 116, A05102
Burlaga, L. F., & Ness, N. F. 2012, ApJ, 749, 13
Burlaga, L. F., Ness, N. F., Acuna, M. H., et al. 2005, Sci, 309, 2027
Burlaga, L. F., Ness, N. F., & Acuna, M. H. 2006, ApJ, 642, 584
Burlaga, L. F., Ness, N. F., & Richardson, J. D. 2003, JGR, 108, 8028
Burlaga, L. F., Ness, N. F., Richardson, J. D., Decker, R. B., & Krimigis, S. M. 2016, ApJ, 818, 147
Cassak, P., Shay, M. A., & Drake, J. F. 2005, PhRvL, 95, 235002
Czechowski, A., Strumik, M., Grygorczuk, J., et al. 2010, A&A, 516, A17
Decker, R. B., Krimigis, S. M., Roelof, E. C., et al. 2005, Sci, 309, 2020
Decker, R. B., Krimigis, S. M., Roelof, E. C., et al. 2008, Natur, 454, 67
Decker, R. B., Krimigis, S. M., Roelof, E. C., & Hill, M. E. 2012, Natur, 489, 124
Drake, J. F., Cassak, P. A., Shay, M. A., Swisdak, M., & Quataert, E. 2009, ApJ, 700, L16
Drake, J. F., Opher, M., Swisdak, M., & Chamoun, J. N. 2010, ApJ, 709, 963
Drake, J. F., Shay, M. A., & Swisdak, M. 2008, PhPl, 15, 042306
Fermo, R. L., Drake, J. F., & Swisdak, M. 2010, PhPl Lett., 17, 010702
Gosling, J. T. 2007, ApJL, 671, L73
Gosling, J. T., Skoug, R. M., McComas, D. J., & Smith, C. W. 2005, JGRA, 110, A01107
Hill, M. E., Decker, R. B., Brown, L. E., et al. 2014, ApJ, 781, 94
Hudson, P. D. 1970, P&SS, 18, 1611
Krimigis, S. M., Roelof, E. C., Decker, R. B., & Hill, M. E. 2011, Natur, 474, 359
Opher, M., Drake, J. F., Swisdak, M., et al. 2011, ApJ, 734, 71
Richardson, J. D., Burlaga, L. F., Decker, R. B., et al. 2013, ApJL, 762, L14
Richardson, J. D., Burlaga, L. F., Drake, J. F., Hill, M. E., & Opher, M. 2016, ApJ, 831, 115
Schoeffler, K. M., Drake, J. F., & Swisdak, M. 2011, ApJ, 743, 70
Schoeffler, K. M., Drake, J. F., & Swisdak, M. 2012, ApJL, 750, 30
Schoeffler, K. M., Drake, J. F., Swisdak, M., & Knizhnik, K. 2013, ApJ, 764, 126
Smith, E. J. 2001, JGR, 106, 15819
Stone, E. C., & Cummings, A. C. 2012, Proc. ICRC, 12, 29
Stone, E. C., Cummings, A. C., McDonald, F. B., et al. 2005, Sci, 309 2017
Stone, E. C., Cummings, A. C., McDonald, F. B., et al. 2013, Sci, 341, 150
Strumik, M., Czechowski, A., Grzedzielski, S., Macek, W. M., & Ratkiewicz, R. 2013, ApJL, 773, L23
Strumik, M., Grzedzielski, S., Czechowski, A., Macek, W. M., & Ratkiewicz, R. 2014, ApJL, 782, L7
Swisdak, M., Drake, J. F., & Opher, M. 2013, ApJL, 774, L8
Wilcox, J. M., & Ness, N. F. 1965, JGR, 70, 5793
Zank, G. P., Hunana, P., Mostafavi, P., et al. 2015, ApJ, 814, 137
Zeiler, A., Biskamp, D., Drake, J. F., et al. 2002, JGR, 107, 1230